Relation between growth procedure and confinement properties of CdSe/ZnSe quantum dots

Ivan-Christophe Robin and Régis André*
CEA-CNRS-UJF "Nanophysics and Semiconductors" Group, Laboratoire de Spectrométrie Physique/CNRS UMR5588, Université J.Fourier, Grenoble, BP87, 38402 St Martin d'Hères, France

Jean-Michel Gérard
CEA-CNRS-UJF "Nanophysics and Semiconductors" Group, Département de Recherche Fondamentale sur la Matière Condensée/SP2M, CEA Grenoble, 17 rue des Martyrs, 38054 Grenoble cedex 9, France
(Received 5 June 2006; revised manuscript received 24 August 2006; published 19 October 2006)

The influence of the growth conditions of CdSe/ZnSe quantum structures on the confinement properties are systematically investigated by time integrated and time resolved photoluminescence. Three samples grown on GaAs (001) by molecular beam epitaxy consisting of three CdSe monolayers embedded between two 40 nm ZnSe barriers are studied. We focus on the influence of the treatment performed after the growth of the strained CdSe layer before capping. The results clearly indicate the formation of quantum dots with excellent optical properties when a specific treatment is performed on the strained CdSe layer before capping, whereas when the CdSe layer is capped directly after growth a rough QW is obtained.

DOI: 10.1103/PhysRevB.74.155318 PACS number(s): 78.67.Hc, 78.66.Hf, 78.55.−m

I. INTRODUCTION

From the applications point of view, the growth of self-assembled semiconductor quantum dots (QDs) was initially motivated by their potential for use in low threshold lasers.[1,2] Then, investigation of CdSe/ZnSe QDs gained considerable attention due to the perspective of incorporating QD structures in laser diodes for the emission in the green and blue-green spectral range.[3–6] In recent years renewed interest in QD systems appeared due to their possible applications as active media in single photon emitters.[7] In particular, self-assembled CdSe/ZnSe QDs is a promising system for single photon emitters in the blue-green range.[8,9]

Self-assembled QDs are formed as a consequence of strain relaxation of a two-dimensional (2D) layer. In the case of CdSe, different methods have been proposed to induce a 2D-3D (three-dimensional) transition of a strained CdSe layer. For example, in Ref. 10, an annealing under selenium flux after the growth of the CdSe layer is used. In this method, the reorganization of the surface into islands is obtained by thermal activation. It was also shown that using thermal activation for the QD formation, higher optical quality and uniformity can be obtained using atomic layer epitaxy (ALE) rather than molecular beam epitaxy (MBE) for the growth of the CdSe layer.[11] Other groups do not use any specific treatment after the growth of the CdSe layer to form QDs.[12–14] In Ref. 12, a 2D-3D transition is observed during the growth by migration enhanced epitaxy (MEE) of the CdSe layer. Long dead times between the exposures to the different elements are used to allow the reorganization of the surface. However, using this method for the growth of the CdSe layer, in Ref. 15, the authors conclude from their results that the QD formation does not occur by Stranski-Krastanov growth mode during CdSe deposition but during capping and only if the ZnSe capping layer is also grown by MEE. They explain the QD formation by a segregation enhanced CdSe reorganization process.[15,16] In order to grow CdSe QDs on ZnSe (001) surfaces, we recently developed a method consisting of covering a layer of strained CdSe with amorphous selenium at low temperature ($\approx -10\ ^\circ$C) by exposing the surface for 15 minutes to a selenium flux of 10^{-6} Torr. This amorphous selenium is then desorbed by ramping the sample temperature from $-10\ ^\circ$C to $280\ ^\circ$C within 15 minutes.[17] The QD formation occurs on the surface during the desorption of the amorphous selenium.[18]

In the present contribution, we investigate the strong differences in the confinement properties between three CdSe/ZnSe heterostructure samples obtained using different procedures to induce a 2D-3D transition of a strained CdSe layer. Those different elaboration procedures lead to different electronic confinement features, ranging from thickness fluctuations along thin quantum wells to purely zero-dimensional (0D) confinement potentials. Those differences have direct consequences on the thermal escape of confined electrons and on the optical properties of the QDs. The confinement properties are studied by means of temperature dependent time-integrated and time-resolved photoluminescence (PL). In particular, our optical measurements clearly indicate that a specific treatment of the strained CdSe layer is needed before capping in order to control the QD formation and minimize electron thermal escape from QDs.

II. SAMPLE ELABORATION

The study we present is based on the optical property comparison between three samples. The three samples consist of three CdSe monolayers (ML) embedded between two 40 nm ZnSe barriers. For all samples, the II-VI growth was started on a deoxidized (001) GaAs substrate following the deoxidation process described in Ref. 19. The oxide was removed without any chemical treatment and no GaAs buffer was grown before the II-VI growth. For all samples, the ZnSe barriers were grown using the same growth procedure with most of the barriers grown by ALE. In particular, for the three samples, after the growth of the first ZnSe barrier and the CdSe layer, the beginning of the capping layer consists of 100 ZnSe ALE cycles. The growth temperature was kept at

 ©2006 The American Physical Society

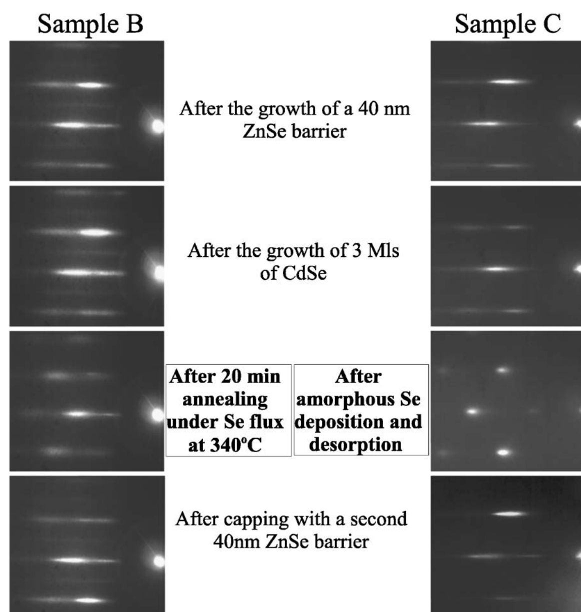

FIG. 1. Comparison of the RHEED patterns between sample B (2D-3D transition induced by thermal activation) and sample C (2D-3D transition induced by the desorption of amorphous selenium) during growth: after the growth of the first ZnSe barrier, after the growth of the CdSe layer, after the 2D-3D transition and after capping.

280 °C for the ZnSe barriers as well as for the CdSe layer. The growth of the CdSe layer was performed by ALE, an ALE cycle consisting of a 10 s exposure to the Cd flux followed by a 10 s dead time, a 10 s exposure to the Se flux and another 10 s dead time. Note that as in Ref. 12 we used long dead times between the exposures to the different elements. One ALE cycle corresponds to the growth of one-half a monolayer of CdSe.[18] What differs between the samples is the treatment done after the CdSe deposition. For sample A, the CdSe layer was capped directly after the growth of 3 CdSe ML, without trying to induce a 2D-3D transition by any specific treatment before capping. For sample B, the sample was annealed at 340 °C for 20 minutes under selenium flux before capping and for sample C, the 2D-3D transition of the strained CdSe layer was induced by deposition of amorphous selenium below room temperature and desorption of this amorphous selenium as described in Ref. 17.

The growth is monitored *in situ* by means of reflection high energy electron diffraction (RHEED).

Figure 1 shows a comparison of the RHEED patterns during the growth of samples B and C at various steps of the growth. When the 2D-3D transition is thermally activated (sample B), we see an evolution of the RHEED pattern during the annealing: some intensity modulation appears along the lines of the initially 2D RHEED pattern. The 2D-3D transition is however much more obvious when amorphous selenium is used to induce the 2D-3D transition: a spotty RHEED pattern is observed after the desorption of amorphous selenium. A spotty RHEED pattern corresponds to a rough surface due to well formed islands.

Figure 1 also shows that our growth procedure allows us to recover a perfectly 2D RHEED pattern corresponding to a smooth surface after the growth of a 40 nm thick ZnSe capping layer.

III. OPTICAL PROPERTIES

The rest of the paper is devoted to the comparison of the optical properties between samples A, B, and C. Before going further, we want to point out the high reproducibility of the samples in terms of optical properties. Samples B and C were chosen as representative of series of samples grown with the same conditions.

Time integrated PL spectra give us interesting features about the localization potentials. In particular we can study this way the size distribution of the QDs, show the existence of a bimodal distribution of QDs or probe the existence of a wetting layer (WL). The temperature dependence of the PL spectra shows how the thermal energy redistributes the carriers into the localization potentials. To better understand the localization into the QDs, time-resolved PL spectra were also studied. Indeed, time-resolved measurements make it possible to precisely investigate the dimensionality of the localization and to quantitatively study the escape of the carriers toward nonradiative channels with temperature.

Time integrated PL spectra were obtained using the 458 nm emission line of an argon laser. Time resolved PL spectra were measured using a frequency-doubled titanium sapphire laser (400 nm) working at a repetition rate of 80 MHz with a pulse width of 150 fs. In this setup the luminescence signal is dispersed by a 0.3 m monochromator equipped with a 300 mm^{-1} grating and time resolved by a streak camera. The spectral resolution is about of 1 meV and the time resolution is 5 ps.

A. Time integrated PL spectra

1. PL spectra at 10 K

Figure 2 compares the time integrated PL spectra at 10 K obtained with the 458 nm line of an argon laser under very low excitation density ($\approx$1 W/cm^2) for the three samples. For such conditions, the excitation is in pseudoresonance with the QDs and the carriers are directly generated into the QDs.

When no treatment of the CdSe layer is performed before capping (sample A), the spectra is well fitted by a single Gaussian centered at 2.49 eV, with a full width at half-maximum (FWHM) of 61 meV. This emission energy is typically the same as the one observed by Gindele *et al.*[13] for QDs obtained using 3.12 CdSe ML grown by MEE and without any specific treatment of the CdSe layer before capping, as described in Ref. 12. A simple confinement model shows that this emission energy corresponds to confinement into a 3 ML thick CdSe quantum well (QW). The large FWHM can be explained by thickness fluctuations of the QW of the order of 1 ML.

We see a clear evolution of the spectra when a treatment is performed on the CdSe layer after growth. When the sample is annealed at 340 °C after the growth of the CdSe layer (sample B), the emission energy shifts toward lower energies. The central emission energy in this case corre-

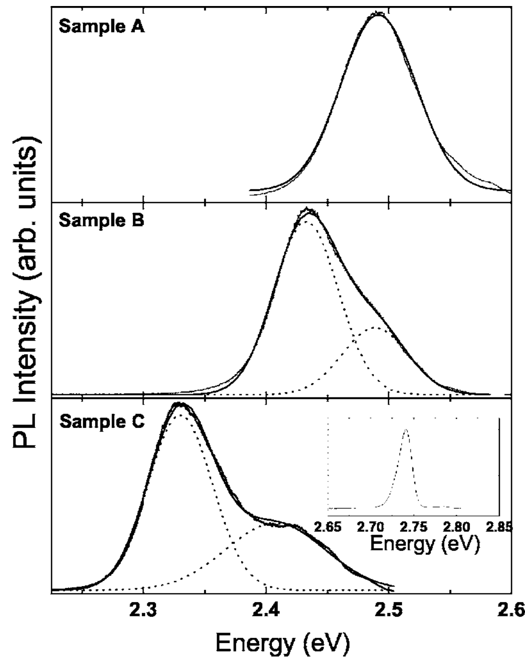

FIG. 2. PL spectra at 10 K obtained with the 458 nm line of an argon laser. The inset shows an emission line observed at 2.74 eV observed for sample C when a doubled titanium sapphire laser at 400 nm is used.

sponds to the one observed in Ref. 10 in which the authors also use annealing under selenium flux to induce a 2D-3D transition of a strained CdSe layer. The PL spectrum can be deconvolved into two Gaussian lines centered at 2.43 eV and 2.48 eV with FWHMs of 51 meV and 54 meV, respectively. This shift toward lower energies is an optical signature of confinement into deeper potentials, corresponding to QD formation. The low energy Gaussian corresponds to QDs. The emission energy of the high energy Gaussian is close to the one observed for sample A. Thus, the high energy Gaussian seems to be due to the emission of a rough QW.

When amorphous selenium is used to induce the 2D-3D transition (sample C), we observed a larger shift toward lower energy, corresponding to confinement into bigger QDs with deeper potentials. As for sample B, the emission spectrum can be deconvolved into two Gaussian lines. The Gaussian lines are centered at 2.33 eV and 2.41 eV with FWHMs of 56 meV and 75 meV, respectively. The emission energies of the two Gaussian lines are at lower energy than the center emission energy of sample A. The two Gaussians are attributed to the emission of two collections of QDs with different average sizes.

For sample C, using a titanium sapphire laser at 400 nm at higher excitation density ($\approx 50\ \mathrm{W/cm^2}$) we observe an emission line at 2.74 eV with a FWHM of 15 meV. This emission is attributed to the emission of a wetting layer (WL). Note that we were able to observe the emission of a WL only for sample C. The emission energy of the WL (2.74 eV) corresponds to a confinement into a 1 ML thick WL. These results show that using amorphous selenium, a clear reorganization of 3 ML of strained CdSe into QDs on a thin WL is obtained. The fact that we can observe the WL is due to the relatively low density of the QDs, estimated to be of $3 \times 10^{10}\ \mathrm{cm^{-2}}$ by atomic force microscopy.[18]

2. Temperature dependence of the PL spectra

The evolution of the PL spectra with temperature gives us interesting informations about the redistribution of carriers in the localization potentials as a function of temperature.

Figure 3(a) shows the evolution with temperature of the PL center emission energy of sample A. The center emission energy was obtained from Gaussian fits. Indeed, the PL spectra of sample A keeps a Gaussian shape up to room temperature. The two continuous lines represent the evolution of the ZnSe band gap as given in Ref. 20. We see that up to 100 K, the emission perfectly follows the ZnSe band gap energy. Above 100 K, the PL emission center energy is at higher energy than the initial evolution. From 220 K, the emission energy follows again the ZnSe band gap evolution, but at an energy 50 meV higher than the initial evolution. So, for temperatures higher than 100 K the carriers begin to be redistributed into potentials emitting at 50 meV higher energy than the levels on which the carrier are localized at low temperatures. In Sec. III B 4, temperature dependent decay-time measurements will show that this behavior is due to a delocalization of the carriers above 100 K into the 2D density of state of the QW, the carriers being localized at low temperature by interface fluctuations of the rough QW [cf. Fig. 3(b)].

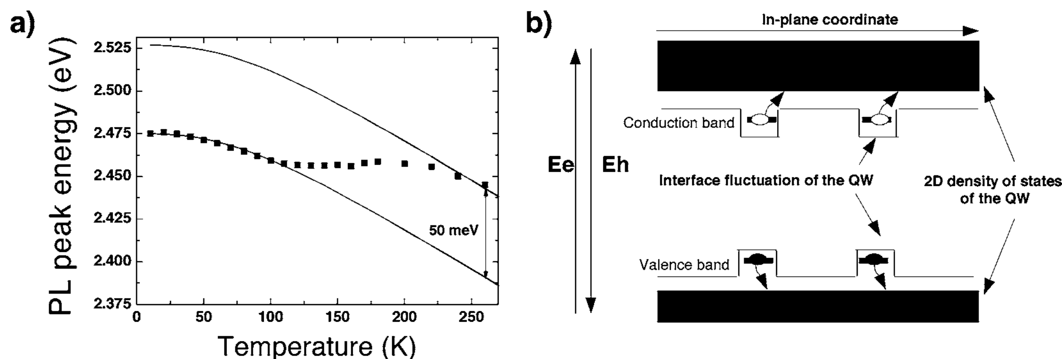

FIG. 3. (a) Evolution of the PL center emission energy of sample A versus temperature. The two solid lines represent the evolution of the ZnSe band gap. (b) Confinement model for sample A: the carriers are localized by interface fluctuations of a rough QW at low temperature and transfer toward the 2D density of states of the QW above 100 K.

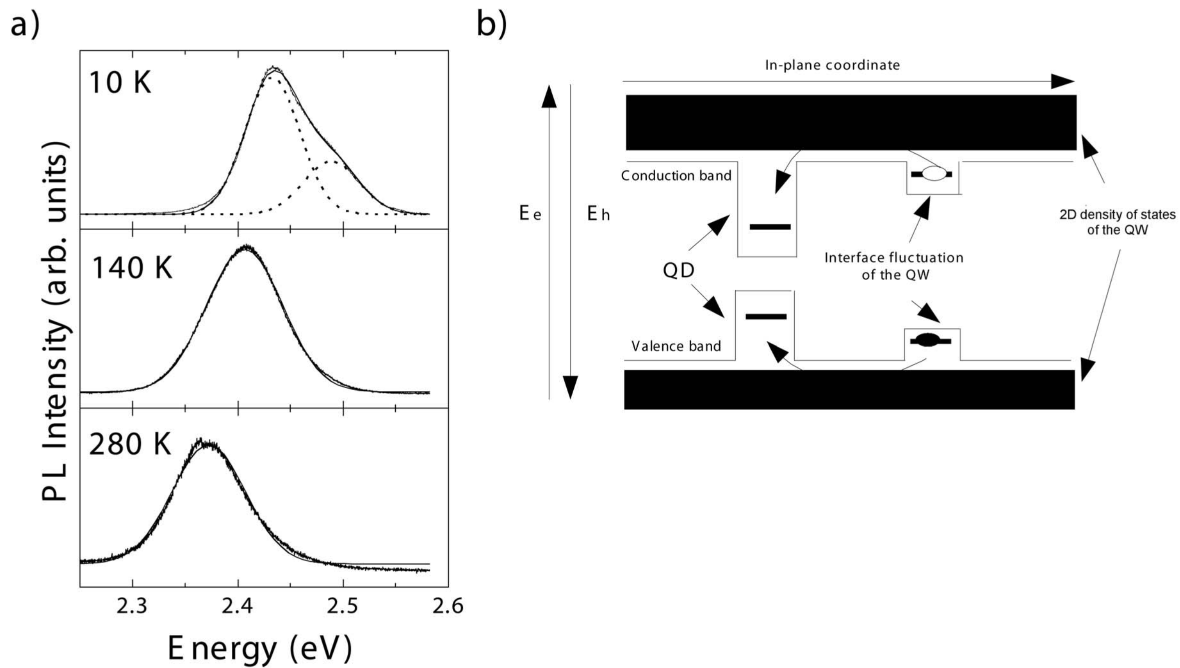

FIG. 4. (a) PL spectra of sample B at 10 K, 140 K, and 280 K. (b) Confinement model of sample B: the carriers localized by interface fluctuations of the rough QW at low temperature (corresponding to the high energy Gaussian), transfer above 100 K toward the QD distribution through the 2D density of states of the QW.

Figure 4(a) shows the PL spectra of sample B measured at 10 K, 140 K, and 280 K. Whereas at 10 K the spectrum can be deconvolved by two Gaussian lines, at 140 K and 280 K, the spectra are well fitted by only one Gaussian line. More precisely the high energy Gaussian disappears around 100 K. In Sec. III A 1 the high energy Gaussian of sample B corresponds to the emission of a rough QW and the low energy Gaussian to the emission of distribution of QD's. In Sec. III B 3, the temperature dependence of the decay times will show that at low temperatures the carriers emitting into the QD line, as well as the carriers emitting into the rough QW line are localized into a 0 D density of states. This suggests that the carriers emitting into the QW are localized on surface fluctuations. The PL spectrum temperature dependence shows that above 100 K, the thermal energy allows the carriers generated into the rough QW and localized by interface fluctuations, to transfer into the deeper localization potentials of the QDs [cf. Fig. 4(b)].

Figure 5 shows the PL spectra of sample C, also measured at 10 K, 140 K, and 280 K. At 10 K the spectrum can be deconvolved into two gaussian lines. As for sample B, the high energy Gaussian disappears around 100 K: Figure 5(a) shows that the spectrum at 140 K is well fitted by a single Gaussian. However the high energy Gaussian reappears in the spectrum at 200 K and Fig. 5(a) shows that the spectrum can clearly be deconvolved again by two Gaussians at 280 K. So, for sample C, from 100 K, the thermal energy transfers the carriers from the high energy QD distribution to the low energy one. Above 200 K, the thermal energy is high enough to thermally redistribute the carriers between the two

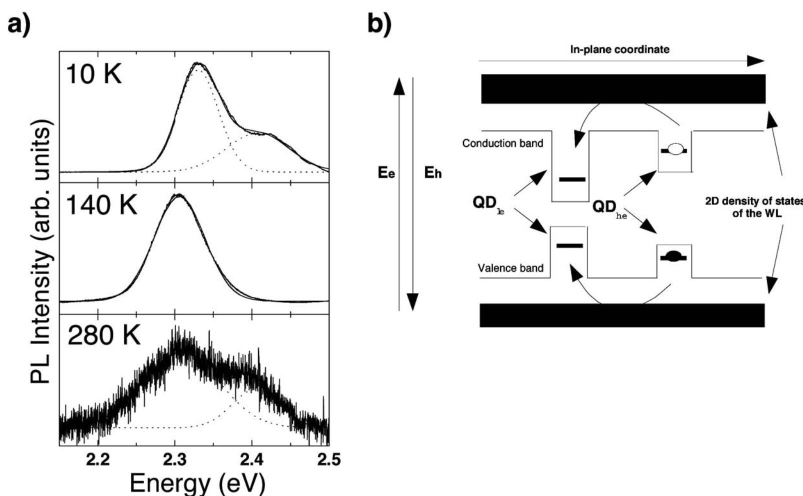

FIG. 5. (a) PL spectra of sample C at 10 K, 140 K, and 280 K. (b) Confinement model of sample C: the carriers localized into the high energy QD distribution (QD_{he}) at low temperature (corresponding to the high energy Gaussian emission), transfer above 100 K toward the low energy QD distribution (QD_{le}) through the 2D density of states of the WL. Above 200 K, the thermal energy is high enough to thermally redistribute the carriers between the two QD distributions.

QD distributions. This behavior is probably due to the fact that from 200 K the thermal energy is high enough to make the carriers reach the high density of states of the WL which is an efficient transfer channel for the carrier between the two QD distributions.

B. PL decay times

Time integrated PL temperature dependence gave us interesting information about the localization potentials for different growth conditions. However, time-resolved PL measurements allow us to better understand the confinement into our heterostructures. Indeed, we can study this way the dimensionality of the confinement, estimate the distance between the confined levels and quantitatively study the escape of the carriers toward nonradiative channels with temperature.

The confinement regime (weak or strong) is also a point of great interest we want to study by the means of time-resolved PL. To see if we are in a strong or in a weak confinement regime we can first compare the lateral confinement size ξ to the Bohr radius a_B of the exciton (a_B=5.6 nm in bulk CdSe). If $\xi << a_B$ we are in a strong confinement regime and if $\xi >> a_B$ we are in a weak confinement regime. It is however difficult to estimate the lateral size of the confinement. In the case of sample A, the carriers are localized on surface fluctuation of a rough QW and the size of those fluctuations is difficult to know. In the case of samples B and C, the diameter of the islands after amorphous selenium desorption is of the order of 20 nm.[18] However capping affects the shape and the composition of the QDs,[16,21,22] so the lateral confinement size is certainly different from the diameter of the islands observed by AFM.

Thus we are going to calculate the theoretical decay time in CdSe QDs in the case of a strong confinement regime. In the next section we will compare this theoretical value to the decay times measured at low temperature, to quantitatively estimate what is the confinement regime in our samples.

The oscillator strength f_η of an optical transition having a direction of polarization $\vec{\eta}$ is given by[23]

$$f_\eta = \frac{2m_0\omega}{\hbar}|\langle f|\vec{\eta}\vec{r}|i\rangle|^2 = \frac{2}{m_0\hbar\omega}|\langle f|\vec{\eta}\vec{p}|i\rangle|^2, \qquad (1)$$

where m_0 is the electron mass, ω the optical transition frequency, i and f the initial and final states of the optical transition, and $\vec{r}$ and $\vec{p}$ are the position and momentum operators. In the case of the strong confinement regime, the oscillator strength can also be written[24] as

$$f_\eta = \frac{\frac{2}{m_0}|\langle u_v(\vec{p})|\vec{\eta}\vec{p}|u_c(\vec{p})\rangle|^2|\langle \Phi_e|\,\Phi_h\rangle|^2}{E} = \frac{E_p|\langle \Phi_e|\,\Phi_h\rangle|^2}{E}, \qquad (2)$$

where $E=\hbar\omega$ is the optical transition energy, u_v and u_c are the Bloch functions in the valence and the conduction bands, Φ_e and Φ_h are the envelope functions of the electron and hole. $E_p=\frac{2}{m_0}|\langle u_v|p_x|u_c\rangle|^2$ (Refs. 25 and 26) is the Kane matrix element, characterizing the optical transition in bulk material. In the case of II-VI materials, $E_p \approx 21$ eV.[26]

From Eq. (1), the oscillator strength can be written using the electrical dipole $\vec{d}=e\vec{r}$,

$$f_\eta = \frac{2m_0\omega}{e^2\hbar}|\langle f|\vec{\eta}e\vec{r}|i\rangle|^2 = \frac{2m_0\omega d_x^2}{e^2\hbar}, \qquad (3)$$

where x is the light direction of polarization and d_x is the dipolar electric operator matrix element along x.

This expression allows us to directly link the oscillator strength to the radiative lifetime in the QDs. Indeed, the radiative lifetime of a QD is given by[24]

$$\frac{1}{\tau} = \frac{d_x^2\omega^3 n}{3\pi\epsilon_0\hbar c^3}, \qquad (4)$$

where n is the CdSe index of refraction. Using Eq. (3), the radiative lifetime reads

$$\frac{1}{\tau} = \frac{f_\eta e^2\omega^2 n}{6\pi m_0 c^3\epsilon_0}. \qquad (5)$$

Using Eq. (2), the radiative lifetime also reads

$$\frac{1}{\tau} = E_p E|\langle \Phi_e|\Phi_h\rangle|^2\frac{e^2 n}{6\pi\hbar^2 m_0 c^3\epsilon_0}. \qquad (6)$$

For an electron and a hole in their lowest s state, $|\langle \Phi_e|\Phi_h\rangle|^2 \approx 1$. Hence we find a radiative lifetime $\tau \approx 400$ ps. For this calculation we did not take into account the Coulomb interaction between the carriers, so when the lateral size of the QD is larger than the Bohr radius in the weak confinement regime, we expect to measure a radiative lifetime shorter than 400 ps.

1. PL decay times at 10 K

To investigate the confinement regime in our samples, we first study the decay time versus the emission energy at 10 K. At this temperature, the measured decay times are the radiative lifetimes of the excitons in the structures. For each emission energy the decay of the luminescence is measured using a 0.5 meV large spectral window.

Figure 6 presents the PL decay times versus the emission energy of samples A, B, and C measured at 10 K. We can see a strong difference in the range of decay times between sample A and samples B and C. For sample A, the decay time varies from 750 ps at the low energy side of the spectrum to 350 ps at the high energy side, whereas for samples B and C the PL decay times are much shorter: between 180 and 330 ps for sample B and between 240 and 300 ps for sample C. The longer decay times for carriers confined in sample A heterostructure show that the overlap of the electron and the hole wave functions is less important than in the case of confinement in samples B and C. This is probably due to the fact that in the case of sample A the carriers are confined by interface fluctuations of a rough QW (cf. Sec. III A 2). In the case of samples B and C the localization into well-defined QDs obtained thanks to a specific treatment of the CdSe layer before capping leads to a better overlap of the wave functions of the electron and the hole and shorter decay times.

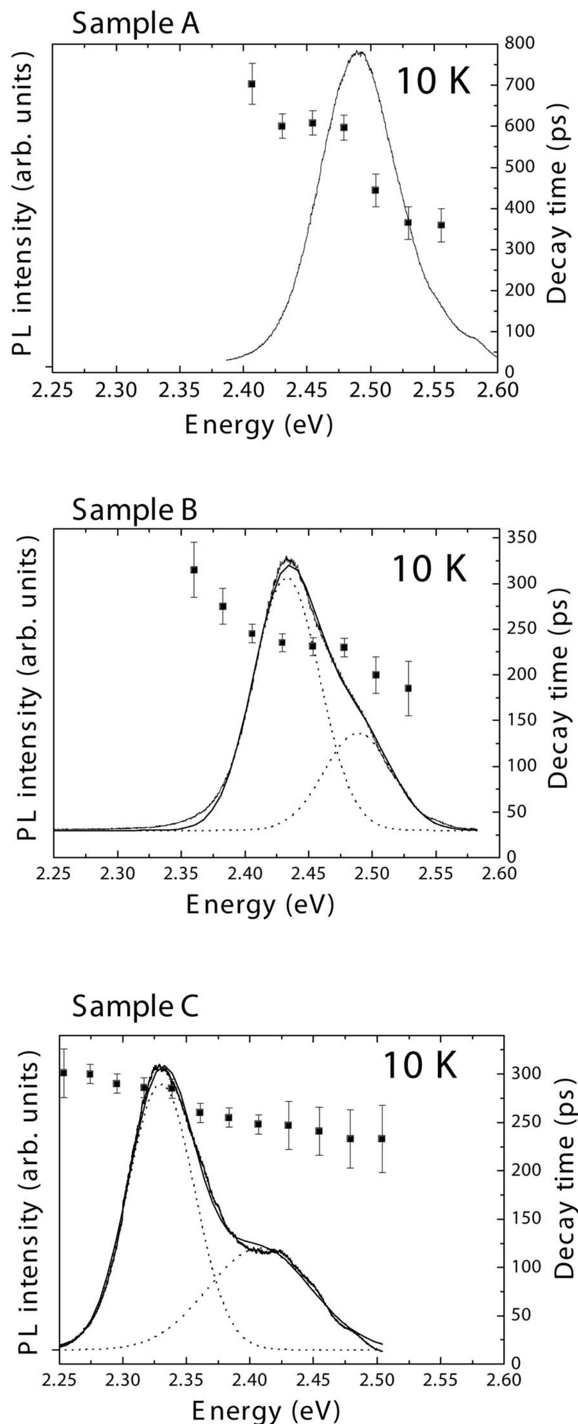

FIG. 6. Decay times versus emission energy for samples A, B, and C measured at 10 K, superimposed on the PL spectra.

The energy dependence of the decay times, with shorter decay times at the high energy side of the spectrum, particularly striking for sample A, with strong variations of the decay times over the PL spectrum was observed by many other groups in CdSe/ZnSe heterostructures, especially when no specific treatment was performed after the growth of the CdSe layer before capping.[13,14,27,28]

In Ref. 13 the increase of the radiative lifetime at lower emission energy was attributed to a decrease of the coherent volume with increasing lateral confinement.[29] This explanation supposes a strong confinement regime at the low energy side of the spectrum and a weak confinement regime at the high energy side. Experimentally, we measure in sample A radiative lifetimes between 350 and 750 ps. If we compare those decay times to the theoretical value of the radiative lifetime calculated in the case of a strong confinement regime (400 ps) we see that in our case we cannot explain decay times as long as 750 ps, even in the case of a strong confinement regime. Long decay times could result from a spatial separation of the electron and the hole due to alloy composition fluctuations. TEM images[21] indicate that in our growth conditions a Cd rich shell can be formed during capping around the CdZnSe heterostructures. Such alloy composition fluctuations could lead to a confinement configuration as shown in Fig. 7. The electron and the hole are confined into the same thickness fluctuation of the rough QW. However, because of its larger mass, the hole can be localized on the Cd rich shell whereas the electron because of its smaller mass is not sensitive to the alloy fluctuation and is localized on a larger scale. In that case, confinement into smaller QW thickness fluctuations leads to a smaller separation of the electron and the hole. Indeed this simple model could also explain the observed smaller decay times at higher energies.

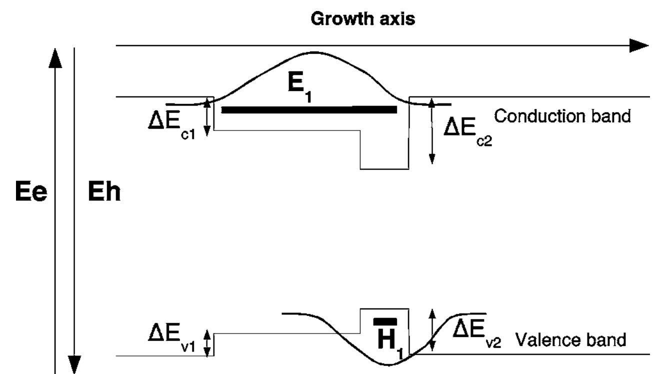

FIG. 7. Separation of the electron and the hole wave functions due to alloy composition fluctuations of a rough QW.

For samples B and C, the measured radiative lifetimes are of the order of 300 ps. For confinement in those samples, the confinement is between the strong and the weak confinement regime: the decay times measured are close to the theoretical value found with the assumption of a strong confinement regime (400 ps), but lower because we did not take into account the Coulomb interaction in our calculations. For sample B, we also observe a strong dependence of the decay times versus the emission energy: the decay times vary from 330 ps at the low energy side of the spectrum to 180 ps at the high energy side. As for this sample the decay times are smaller than 400 ps, the energy dependence of the decay times can effectively be explained by a change of the coherent volume as suggested in Ref. 13: the confinement into interface fluctuation is less deep than the confinement into QDs (this is why the emission of the rough QW is observed at higher energy than the QD emission). The lateral size of the interface fluctuations can also be larger than the lateral size of the QDs and we then obtain a weak confinement regime for the interface fluctuations emitting a higher energy

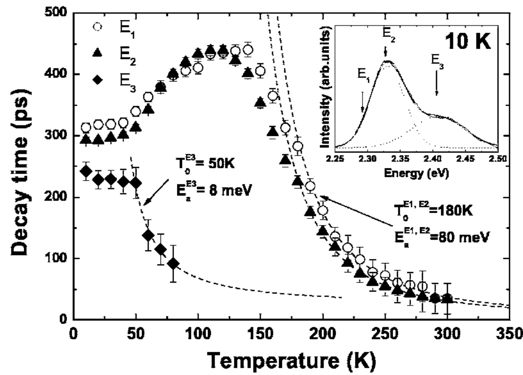

FIG. 8. Decay time temperature dependence of sample C for three spectral positions. The inset shows the PL spectrum at 10 K. The arrows indicate the three spectral positions studied.

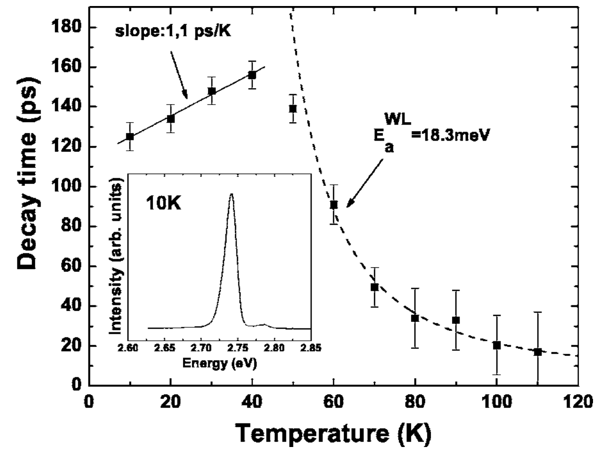

FIG. 9. Temperature dependence of the decay time of the WL of sample C. The inset shows the PL spectra of the WL at 10 K.

with short decay times whereas a stronger confinement regime and larger decay times are obtained for the QDs emitting at lower energy.

For sample C, the decay time is quasiconstant over each Gaussian component of the spectrum: about 300 ps for the low energy Gaussian and 250 ps for the high energy Gaussian. This is certainly due to the fact that the two Gaussians correspond to the emission of two different types of well-defined QDs, each QD distribution having its specific properties.

2. Temperature dependence of PL decay times of sample C

To better understand the confinement in our heterostructures, the evolution with temperature of the PL decay times is studied. Temperature dependence of the PL decay time is a signature of the confinement dimensionality. To extract more information from this study, for each sample a theoretical model is used to fit the experimental temperature dependence of the decay times. This model, that we are going to present in this section allows us to understand the redistribution of the carriers with temperature into the different confined levels, to determine which levels play a role into the emission process, to estimate the energy separation between the confined levels and to better understand the escape of the carriers with temperature toward nonradiative channels. For clarity, especially for the introduction of the model used to fit the temperature dependence of the decay times, we will first focus on sample C.

Micro-PL measurements (not shown) show that the emission energy of a single QD follows with temperature the ZnSe band-gap evolution given in Ref. 20. Thus, to be sure to study the same QDs over the whole temperature range, the spectral window used to measure the decay times is shifted with temperature following the ZnSe band-gap evolution.

Figure 8 presents the temperature dependence of PL decay time of sample C for three different spectral positions. The spectral positions E_1 and E_2 correspond to the low energy tail and the maximum of the low energy Gaussian. For these emission energies we were able to measure the decay times up to room temperature. The spectral position E_3 corresponds to the maximum of the high energy Gaussian. For this emission energy we could measure the decay time up to 90 K. As we saw in Sec. III A 2, for higher temperatures, the emission of the high energy Gaussian disappears.

The temperature dependence of the decay time is determined by the thermalization effect and is known to reflect the dimensionality of quantum structures.[30–32] For the three emission energies, the decay times do not vary with temperature between 10 K and 50 K. This is due to the zero-dimensional confinement into the QDs: the thermalization is suppressed because of the δ-function-like density of states.

For the high energy Gaussian, we observe an exponential decrease of the decay time above $T_0^{E3}=50$ K, which corresponds to the activation of the nonradiative channels. The activation energy of the nonradiative channels is $E_a^{E3}=8$ meV for this QD distribution.

We see that for the two emission energies within the low energy Gaussian, the temperature dependence of the decay times is the same, showing that the confinement characteristics are the same within the same QD distribution. Between 60 K and 140 K we observe an increase of the decay times from 300 ps to 450 ps. In Ref. 33 an increase of the decay time with temperature was also measured on a single CdSe QD. Using a quantitative model we will explain this increase of the decay times by a thermalization of the carriers on the excited states of the QDs. Above 150 K the decay time decreases because the carriers begin to reach the nonradiative channels. Above $T_0^{E1}=T_0^{E2}=180$ K we then observe an exponential decrease of the decay times, the nonradiative channels being dominant in the deexcitation process. The activation energy of the nonradiative channels for the two emission energies studied is $E_a^{E1,E2}=80$ meV.

We also measured the PL decay time versus the temperature on the WL of sample C. The results are shown in Fig. 9. We observe a linear increase of the decay time between 10 and 40 K with a slope of 1,1 ps/K. This behavior is a signature of a confinement into a two-dimensional structure[30] and was reported before in the case of GaAs/GaAlAs QWs (Refs. 34 and 35) and CdTe QWs.[36] The temperature dependent PL decay clearly shows that the emission observed around 2.75 eV for sample C is due to a WL. More precisely, for a two-dimensional confinement, the linear dependence of the radiative lifetime reads[30]

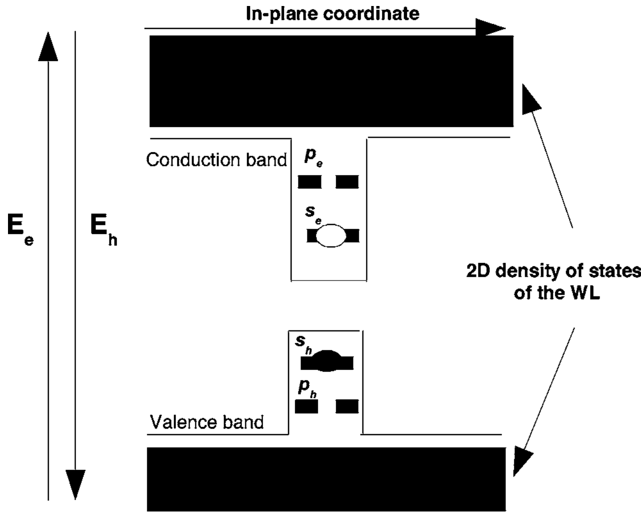

FIG. 10. Schematic of the model used to explain the QD distribution decay time temperature dependence.

$$\tau_r(T) = \frac{\tau_0 k_B T}{E^X_{\text{cinmax}}}, \tag{7}$$

where $\tau_0 = 1/\Gamma_0$ is the radiative lifetime for $k_\parallel = 0$. This radiative lifetime is linked to the FWHM of the zero-phonon excitonic line by the Heisenberg uncertainty relation $\Delta E \tau_0 = \hbar$. In Eq. (7), E^X_{cinmax} is the maximal kinetic energy of the excitons that recombine radiatively,

$$E^X_{\text{cinmax}} = \frac{\hbar^2 k^2_{\parallel\max}}{2M}, \tag{8}$$

where M is the exciton mass and $k_{\parallel\max}$ the maximum in-plane wavevector of the excitons that recombine radiatively. $k_{\parallel\max}$ is linked to the emission energy by the equation

$$\hbar k_{\parallel\max} = n \frac{E_{\text{PL}}}{c}, \tag{9}$$

where n is the ZnSe index of refraction and E_{PL} is the WL emission energy.

Using those equations and the slope value (1.1 ps/K) for the linear temperature dependence of the decay time, we find $\tau_0 = 2.5$ ps, which corresponds to a zero-phonon FWHM line $\Gamma_0 = 260$ μeV. In Ref. 37 Γ_0 values of about 200 μeV are measured by reflectivity in ZnSe based QWs. In Ref. 38 a value of Γ_0 of 300 μeV is deduced from a Rabi splitting measurement in the strong coupling regime in CdZnSe QWs. Those values are in good agreement with the Γ_0 value we find from the decay time temperature dependence of the WL.

We will now present a model to explain the temperature dependence of the decay time of the low energy QD distribution. In particular, we will show that the increase of the decay times between 60 K and 140 K is compatible with confinement into QDs. This model is similar to the one presented in Ref. 39 to explain decay time temperature dependent of CdTe QDs. A schematic of the model is shown in Fig. 10. It is based on a thermal redistribution of an electron and a hole over the discrete states of a QD and the 2D continuum states of the WL. We will consider the redistribution of the electron and the hole separately, assuming that the Coulomb effects are negligible compared to the confinement effects. This assumption is reasonable according to the calculation done in Sec. III B 1 which showed us that we are close to the strong confinement regime in our QDs.

The decay time measurements on the QD distribution were done under very weak excitation with no more than one exciton in a QD. This is why we consider a QD occupied by one electron and one hole. We consider a lowest s state and two excited p states for the electron e and the hole h. We also consider the continuum density of states of the WL $D^{wl}_{e(h)} = \frac{m_{e(h)} L^2}{\pi \hbar^2}$ where L^2 is the typical area accessible for a continuum state wave function and $m_{e(h)}$ the electron (hole) mass.

For a QD containing one exciton, the sum over all the level occupation probabilities for the electron (and the hole) must be unity,

$$\int dE D_{e(h)}(E) p_{e(h)}(E) = 1, \tag{10}$$

$D_{e(h)}(E)$ is the electron (hole) density of states and $p_{e(h)}(E) = \frac{1}{Z_{e(h)}} \exp(-E/k_B T)$ is the canonical occupation probability.

Taking the QD s-state energy as origin, $E^p_{e(h)}$ the energy of the p states and $E^{wl}_{e(h)}$ the lowest energy of the WL continuum density of states, $D_{e(h)}(E)$ reads

$$D_{e(h)} = 2\delta(E) + 4\delta(E - E^p_{e(h)}) + D^{wl}_{e(h)} \Theta(E - E^{nr}_{e(h)}). \tag{11}$$

Θ being the Heaviside function. From Eq. (10) we can determine the partition function $Z_{e(h)}$ versus temperature

$$Z_{e(h)}(T) = 2 + 4 \exp(-E^p_{e(h)}/k_B T) + k_B T D^{wl}_{e(h)} \exp(-E^{wl}_{e(h)}/k_B T). \tag{12}$$

Then we obtain the occupation probabilities $e_s(h_s)$ of the s orbital as well as the occupation probability $e_p(h_p)$ of one of the two p orbitals,

$$e_s(h_s) = 2p_{e(h)}(0) = \frac{2}{Z_{e(h)}(T)},$$

$$e_p(h_p) = 2p_{e(h)}(E^p_{e(h)}) = \frac{2 \exp(-E^p_{e(h)}/k_B T)}{Z_{e(h)}(T)}. \tag{13}$$

The two factors are due to the spin degeneracy.

The probability of an electron (or hole) being in the WL is given by

$$e_{wl}(h_{wl}) = \int_{E^{wl}_{e(h)}}^{\infty} D^{wl}_{e(h)} p_{e(h)}(E) dE = D^{wl}_{e(h)} k_B T \cdot \frac{\exp(-E^{wl}_{e(h)}/k_B T)}{Z_{e(h)}(T)}. \tag{14}$$

We then consider three different recombination channels: (i) and (ii) discrete recombinations between electrons and holes in an s or in a p orbital with lifetimes τ_s and τ_p, respectively; (iii) nonradiative recombination that will occur

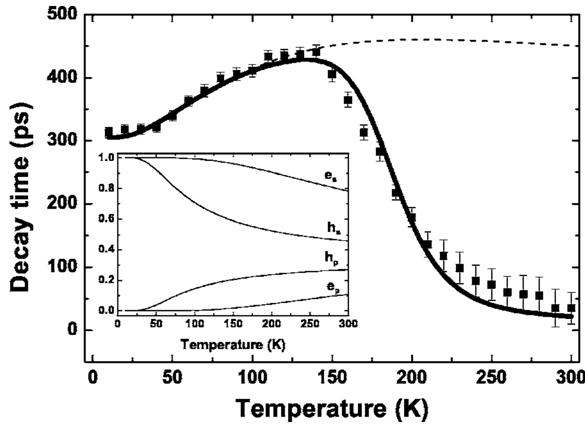

FIG. 11. Measured (datapoints) and calculated (curves) decay time temperature dependence of the low energy QD distribution of sample C. The dotted curve presents the evolution of the calculated decay time when the nonradiative channels are not taken into account. The inset presents the temperature dependence of the occupation probabilities e_s, h_s, e_p, and h_p of the electron and the hole into the s orbital or into one of the two p orbitals when the escape of the carriers toward the WL is not taken into account.

with a nonradiative lifetime τ_{nr} if the electron or the hole reach the WL. Thus the decay time τ reads

$$\frac{1}{\tau} = \frac{e_s h_s}{\tau_s} + 2\frac{e_p h_p}{\tau_p} + \frac{(e_{wl} + h_{wl})}{\tau_{\mathrm{nr}}}. \qquad (15)$$

We calculate the energy separation between the s state and the p states considering a parabolic confinement potential in the QD.[40] Thus, the lateral dimension $L_{x,y}$ is then an adjustable parameter of the model. The energy separation between the s state and the WL continuum density of states is fixed, given the energy separation between the emission of the QD distribution and the emission of the WL.

Figure 11 presents the measured (datapoints) and calculated (curves) decay time temperature dependence of the low energy QD distribution. The dotted curve presents the evolution of the decay times when the nonradiative recombinations are not taken into account (in this calculation we suppressed the escape of the carriers toward the WL). We see that we can perfectly reproduce the temperature dependence of the decay times only considering the radiative recombination processes up to 140 K. The s state and the p states radiative lifetimes are found to be $\tau_s = 305$ ps and $\tau_p = 250$ ps. The energy separation between the s state and the p correspond to a lateral size of the QD $L_{xy} = 7.3$ nm. The inset of Fig. 11 presents the temperature dependence of the occupation probabilities e_s, h_s, e_p, and h_p of the electron and hole s and P orbitals when the escape of the carriers toward the WL is not taken into account. We see that the increase of the decay times between 60 K and 140 K can be explained by a thermal redistribution of the hole in p states at low temperature, the electron remaining in the lowest s state.

Discussion: This model gives us a lateral size of the confinement into our QDs smaller than the diameter of the islands measured by AFM [typically 20 nm (Ref. 18)]. As suggested in Refs. 15 and 16 this tends to show that capping modifies the shape and the size of the QDs. The confinement lateral size (7.3 nm) is close to the Bohr radius of the exciton (5.6 nm in bulk CdSe), showing that we are close to a strong coupling regime, which justifies the approach used in the model. We also find similar lifetimes for recombination into an s state or into a p state. This is consistent with the fact that the overlap of the wave functions of the electron and the hole is of the same order of magnitude when the two carriers are in orbitals with the same symmetry.

However, with this model we are not able to perfectly reproduce the exponential decrease of the decay times on the high temperature side. This is due to the fact that the only nonradiative process we consider is the escape of the carriers toward the WL. More precisely, the activation energy we calculate is greater than the one measured. This is due to the fact that we fixed the energy separation between the s states and the WL. However, defects in the ZnSe barriers must also play a role in the nonradiative recombinations. The defects in the barriers are also easier to reach when the thermal energy redistributes the carriers into p states because when the carriers are localized on excited levels, their wave functions penetrate deeper into the barriers. We must take into account other nonradiative channels than the WL.

The activation energy we measure is 80 meV. In Fig. 12 we present the result of a calculation using a nonradiative density of states for the holes D_h^{nr} 80 meV higher than the s state of the QD. The Arrhenius plot of the measured and calculated decay time vs the inverse of the temperature presented in the inset of Fig. 12 shows that in this case we are able to perfectly reproduce the exponential decay. Thus, the model fits now very well the evaluated activation energy. Note that even if we obtain a good fit, we cannot however quantitatively identify the defects which play a role into the nonradiative process: this model just tells us that the WL is not the only nonradiative escape channel.

3. PL decay time temperature dependence of sample B

Figure 13 presents the evolution of the PL decay times of sample B for three different spectral positions. The spectral positions E_1 and E_2 correspond to the low energy tail and the maximum of the low energy Gaussian. The spectral position E_3 corresponds to the maximum of the high energy Gaussian. For this emission energy we could measure the decay time up to 150 K, the emission of the high energy Gaussian disappearing for higher temperatures.

For the three emission energies, the decay times do not vary with temperature between 10 K and 50 K. As for sample C, we observe a zero-dimensional confinement at low temperature. In Sec. III A 1, from the comparison between the emission energy of the high energy Gaussian of sample B and the emission energy of sample A, we concluded that the high energy Gaussian in the spectrum of sample B is probably due to a rough QW. In this case, the zero-dimensional confinement is due to localization of the carriers by interface fluctuations. For the high energy Gaussian, we observe an exponential decrease of the decay time above $T_0^{E3} = 80$ K, which corresponds to the activation of the nonradiative channels. The activation energy of the nonradiative channels is $E_a^{E3} = 14$ meV.

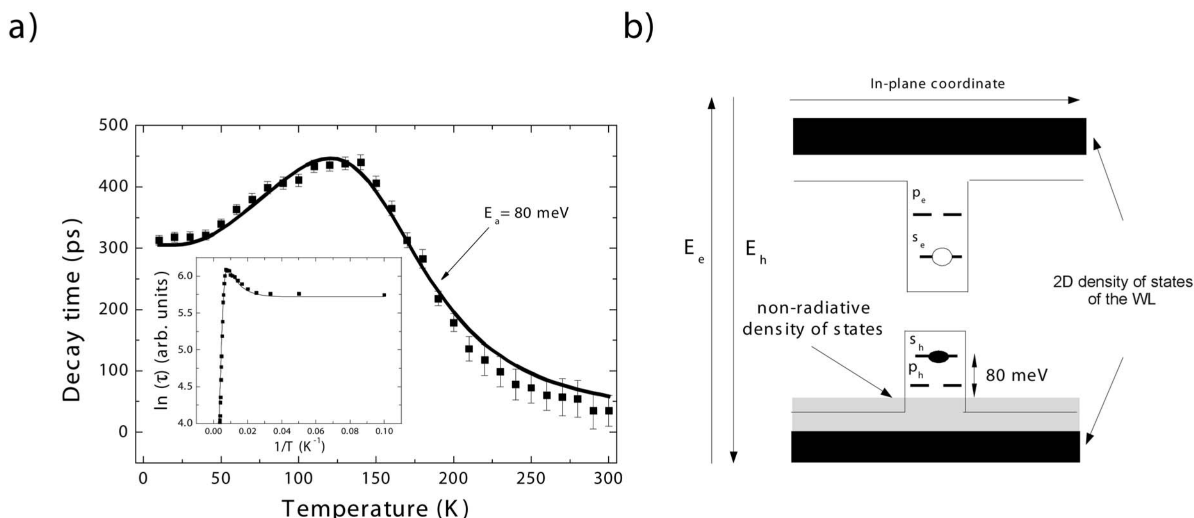

FIG. 12. (a) Measured (datapoints) and calculated (curve) temperature-dependent decay times of the low energy QD distribution of sample C. The inset shows an Arrhenius plot of the measured and calculated decay times vs 1/T. (b) Schematic of the model used for this calculation: we introduced a nonradiative density of states for the holes corresponding to defects into the ZnSe barriers.

For the two emission energies of the low energy Gaussian, the evolutions of the decay time with temperature are similar. Between 50 K and 160 K we observe an increase of the decay times from about 250 ps to 350 ps. Above 160 K we observe a decrease of the decay times which becomes exponential from $T_0^{E_1}=T_0^{E_2}=200$ K with an activation energy $E_a^{E_1,E_2}=135$ meV. Compared to sample C the increase of the decay time is less important. This is certainly due to the fact that the carriers are confined into QDs with larger lateral size: the energy separation between the p states and the s states is more important and a higher thermal energy is then needed to reach the p states. The same model we applied for sample C will confirm this interpretation. We also note that the temperature T_0 for which the nonradiative deexcitation processes become dominant and the corresponding activation energy is higher than for sample C. This could be due to the fact that for sample B, the redistribution of the carriers on p states is less important than for sample C so the probability for a carrier to reach a defect into the barriers is lower.

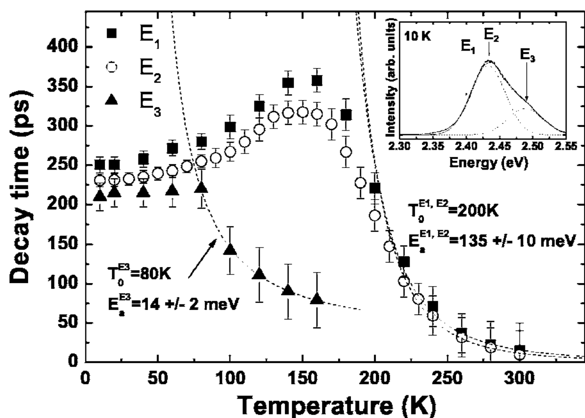

FIG. 13. Decay time temperature dependence of sample B for three spectral positions. The inset shows the PL spectrum at 10 K. The arrows indicate the three spectral positions studied.

Figure 14 presents the best fit of the low energy Gaussian decay time temperature dependence. We used the same model as the one presented in Sec. III B 2. The redistribution with temperature of the electron and the hole in s and p states is calculated separately. To fit the exponential decay at high temperature, we introduced a nonradiative density of states D_{nr} for the holes 135 meV higher than the s state of the QD corresponding to defects into the barrier. We see that for this sample also we can perfectly fit the increase of the decay times. As for sample C, this increase is due to a redistribution of the hole in p states, the electron remaining in the lowest s state. The energy separation between the s states and the p states corresponds in this case to a lateral size of the QD $L_{x,y}=11$ nm. Therefore this model shows that for sample B, the carriers are confined into QDs with larger lateral size than for sample C. This can also explain the shorter decay times we measure at low temperature on sample B. The

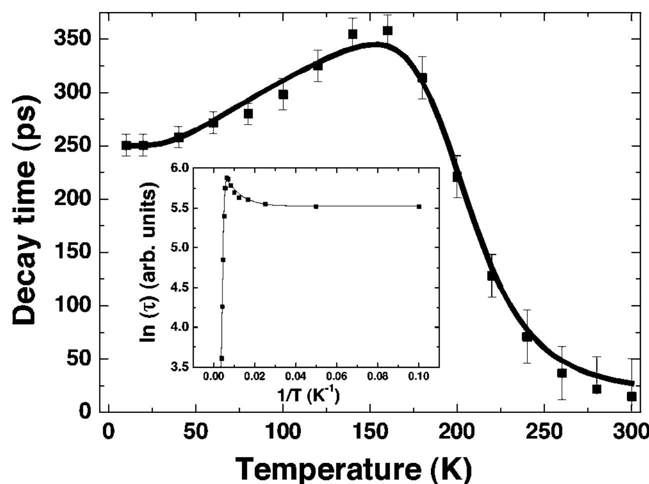

FIG. 14. Measured (datapoints) and calculated (curve) temperature-dependence decay times of the low energy Gaussian of sample B. The inset shows an Arrhenius plot of the same data.

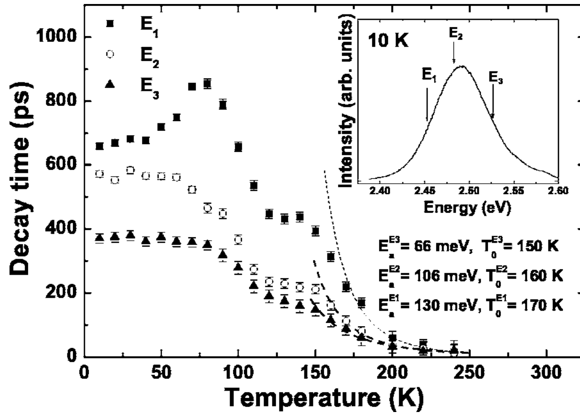

FIG. 15. Decay time temperature dependence of sample A for three spectral positions. The inset shows the PL spectrum at 10 K. The arrows indicate the three spectral positions studied.

Arrhenius plot presented in the inset of Fig. 14 shows that the model fits very well the evaluated activation energy.

4. PL decay time temperature dependence of sample A

Figure 15 presents the evolution with temperature of the PL decay times of sample A for three different spectral positions. The spectral positions correspond to the low energy tail, the maximum and the high energy tail of the spectrum. The temperature dependence of the decay times is different for each emission energy. However, for the three spectral positions, the decay time is constant between 0 and 40 K, showing that even if we did not try to induce a 2D-3D transition for this sample, the carriers are localized on discrete energy levels at low temperature. The discrete density of states is certainly due to the interface fluctuations of a rough QW.

For the low emission energy (E_1), we see an increase of the decay time from 700 ps to 860 ps between 50 K and 80 K. For the two other emission energies, the decay time is constant to about 90 K. For the three emission energies, we then observe a decrease of the decay times between 90 K and 120 K. What is striking about this sample is the fact that the decay time becomes constant again for the three emission energies between 120 K and 140 K. Above about 150 K, we then observe an exponential decrease of the decay times.

In Sec. III A 2, the temperature dependence of the PL center emission energy showed us that the carriers are redistributed above 100 K in potentials 50 meV higher than the levels on which the carriers are localized at low temperature. We interpreted this behavior by a delocalization of the carriers above 100 K into the 2D density of states of the QW, the carriers being localized by thickness fluctuations at low temperature. The model we will present shows that the plateau in decay times between 120 K and 140 K is another signature of the redistribution of the carriers into the QW above 100 K.

To explain our observations, we will present a model similar to the one presented in Sec. III B 2. We were not able to explain the decay time temperature dependence of sample A with a discrete density of state for the confined levels. The plateau observed between 120 K and 140 K is certainly due to a localization on excited levels at high temperature. In this case, only a high density of states such as the 2D density of state of the QW can allow an occupation rate close to 1 at higher temperature into other levels than the fundamental level.

In Secs. III B 2 and III B 3 we explained the increase of the decay time observed for the low energy Gaussians of samples C and B by a thermally activated redistribution of the electron and the hole into p states separately. For sample A, at the high energy side of the spectrum, we do not observe an increase of the decay times and we deduced from this observation that we have an excitonic behavior of the carriers at high emission energy. Indeed, for this sample, the confinement by interface fluctuations of a rough QW is certainly weaker than in the case of confinement into QDs and a weak confinement favors exciton formation.

For the emission energies E_2 and E_3, we consider the evolution of an exciton on an s fundamental level and a 2D continuum with a density of state D_{ex}^{2D}. To model the nonradiative recombinations we also consider a nonradiative density of states D_{ex}^{nr}. The exciton density of states then reads

$$D_{ex} = 2\delta(E) + D_{ex}^{2D}\Theta(E - E_{ex}^{2D}) + D_{ex}^{nr}\Theta(E - E_{ex}^{nr}). \quad (16)$$

E_{ex}^{2D} and E_{ex}^{nr} being the energy separations between the fundamental s state and the 2D continuum and the nonradiative states, respectively.

The partition function of the exciton is

$$Z_{ex}(T) = 2 + k_B T D_{ex}^{2D} \exp(-E_{ex}^{2D}/k_B T) + k_B T D_{ex}^{nr} \times \exp(-E_{ex}^{nr}/k_B T). \quad (17)$$

The occupation probabilities ex_s of the s orbital and the occupation probabilities ex_{2D} and ex_{nr} of the 2D and the nonradiative contimua are

$$ex_s = \frac{2}{Z_{ex}(T)},$$

$$ex_{2D} = D_{ex}^{2D} k_B T \frac{\exp(-E_{ex}^{2D}/k_B T)}{Z_{ex}(T)},$$

$$ex_{nr} = D_{ex}^{nr} k_B T \frac{\exp(-E_{ex}^{nr}/k_B T)}{Z_{ex}(T)}. \quad (18)$$

Considering a radiative lifetime τ_s for a recombination on the s state, a radiative lifetime $\tau_{2D}(T)$ for a recombination into the 2D density of states and a nonradiative lifetime τ_{nr}, the decay time τ reads

$$\frac{1}{\tau} = \frac{ex_s}{\tau_s} + \frac{ex_{2D}}{\tau_{2D}(T)} + \frac{ex_{nr}}{\tau_{nr}}. \quad (19)$$

For recombination into the 2D density of states, we considered the same linear temperature dependence of the decay time $\tau_{2D}(T)$ as we measured on the 2D WL of sample C, i.e., 1.1 ps/K. For the energy separation E_{ex}^{2D} between the s fundamental state and the 2D density of states, we used the

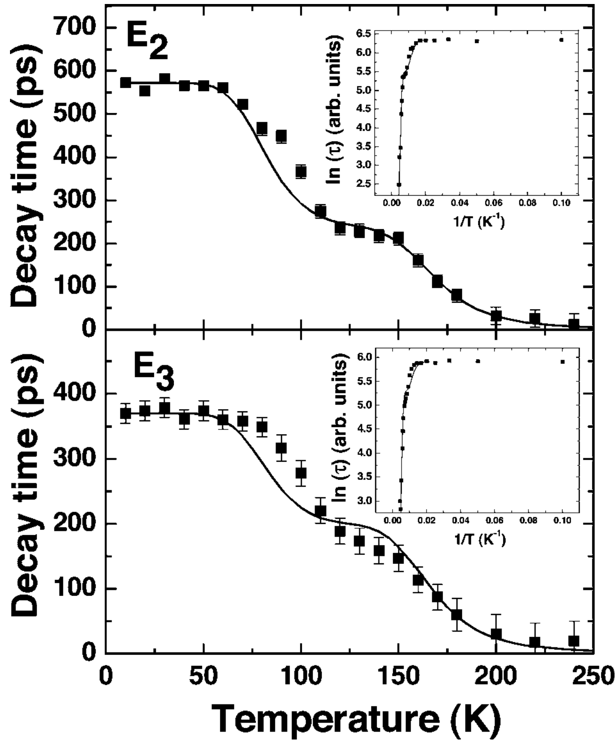

FIG. 16. Measured (datapoints) and calculated (curves) temperature-dependence decay times of sample C for the two emission energies E_2 and E_3. The insets show Arrhenius plots of the same data.

value measured from the temperature dependence of the PL emission energy in Sec. III A 2, i.e., 50 meV.

Figure 16 presents the best decay time fits we obtained for the emission energies E_2 and E_3 by adjusting D_{ex}^{2D}, D_{ex}^{nr}, E_{ex}^{nr}, and τ_{nr}. Note that the values of E_{ex}^{2D} (=50 meV), D_{ex}^{2D}, D_{ex}^{nr}, and τ_{nr} are the same for the two fits. The energy separation E_{ex}^{nr} between the fundamental s state and the nonradiative continuum was changed according to the energy difference between E_2 and E_3. The only difference between the two fits is the s radiative lifetime τ_s. This lifetime corresponds to the one measured at 10 K for each emission energy, i.e., τ_s =570 ps for E_2 and τ_s=370 ps for E_3. We see that we can reach a fairly good agreement between the calculated curves and the experimental data. According to this model, the plateau in decay times observed between 120 K and 140 K is indeed due to a delocalization of the exciton into a 2D density of states.

An excitonic model cannot however explain the temperature dependence of the decay time observed for the emission energy E_1, especially the increase of the decay time observed between 50 and 80 K. For this emission energy, the Coulomb interaction between the electron and the hole must be too weak to form an exciton. Indeed, E_1 corresponds to the low energy tail of the spectrum and if the long decay time is due to the separation of the electron and the hole as described in Fig. 7, this separation is the most important on the low energy side of the spectrum. We used the model described in Sec. III B 2 for this emission energy. We treated the electron and the hole separately, introducing a 2D density of states and a nonradiative density of states for each carrier. We

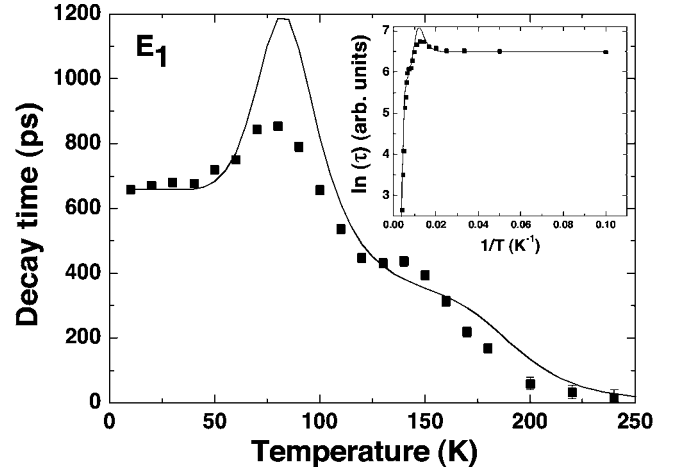

FIG. 17. Measured (datapoints) and calculated (curve) temperature-dependence decay times of sample C for the emission energy E_1. The inset shows an Arrhenius plot of the same data.

chose the energies separation $E_{e(h)}^{2D}$ between the s states and the 2D densities of states for the electron and the hole so that $E_e^{2D}+E_h^{2D}$=50 meV. We also took the same density of states for the 2D continuum and nonradiative channels as for the calculations done for the emission energies E_2 and E_3.

There are some quantitative discrepancies between the measured and the calculated curves (Fig. 17). However, considering the simplicity of the model and the fact that we tried to minimize the number of parameters as much as possible, we see that we obtain a good qualitative agreement over the whole temperature range. In particular, this calculation also shows a plateau around 130 K which is due to a delocalization of the electron and the hole into a 2D density of states. Note that for this sample also, the Arrhenius plots presented in the insets of Figs. 16 and 17 show that the model fits very well the evaluated activation energies.

IV. CONCLUSION

We studied the relation between the confinement properties and the growth procedure to form CdSe/ZnSe QDs. Three samples have been studied, each sample corresponding to a different treatment of the strained CdSe layer before capping. Our study clearly shows that to control the localization of the carriers into QDs, a specific treatment is needed after the growth of the CdSe layer before capping. The optical properties of the heterostructures strongly depend on the treatment performed. The energy shift toward low energies measured by time-integrated PL measurements gives clear evidence that the carriers are localized into deeper localization potentials when a specific treatment is performed before capping. The lowest emission energy, corresponding to localization into QDs, is observed when amorphous selenium is used to induce the 2D-3D transition (sample C). In this case, the emission from the WL is observed for higher excitation density. When no treatment is performed before capping, long decay times are measured at low temperature with strong variation versus the emission energy due to the separation of the electron and the hole in a rough QW. Tempera-

ture dependent PL measurements show that the carriers are in this case localized on interface fluctuations at low temperature and are delocalized into the 2D density of states of the QW at higher temperature. Using a specific treatment before capping much shorter decay times at low temperature are obtained, corresponding to localization into QDs. The localization into QDs can be maintained up to 200 K. Temperature dependent PL measurements show that the redistribution into excited levels of the QDs with temperature as well as the quality of the barriers play an important role in the escape of the carriers toward nonradiative channels.

ACKNOWLEDGMENTS

The authors thank H. Mariette, K. Kheng, S. Moehl, J. Bleuse, Le Si Dang, C. Bougerol, S. Tatarenko, and T. Tiedje for their help and fruitful discussions.

---

*Electronic address: regis.andre@ujf-grenoble.fr

[1] Y. Arakawa and H. Sakaki, Appl. Phys. Lett. **40**, 939 (1982).

[2] M. Asada, Y. Miyamoto, and Y. Suematsu, IEEE J. Quantum Electron. **22**, 1915 (1986).

[3] N. N. Ledentsov, I. L. Krestnikov, M. V. Maximov, S. V. Ivanov, S. L. Sorokin, P. S. Kop'ev, Z. I. Alferov, D. Bimberg, and C. M. S. Torres, Appl. Phys. Lett. **69**, 1343 (1996).

[4] N. N. Ledentsov, I. L. Krestnikov, M. V. Maximov, S. V. Ivanov, S. L. Sorokin, P. S. Kop'ev, Z. I. Alferov, D. Bimberg, and C. M. S. Torres, Appl. Phys. Lett. **70**, 2766 (1996).

[5] M. Strassburg *et al.*, Appl. Phys. Lett. **72**, 942 (1998).

[6] S. V. Ivanov *et al.*, Appl. Phys. Lett. **74**, 498 (1999).

[7] E. Moreau, I. Robert, J. M. Gérard, I. Abram, L. Manin, and V. Thierry-Mieg, Appl. Phys. Lett. **79**, 2865 (2001).

[8] K. Sebald, P. Michler, T. Passow, D. Hommel, G. Bacher, and A. Forchel, Appl. Phys. Lett. **81**, 2920 (2002).

[9] I. C. Robin, R. André, A. Balocchi, S. Carayon, S. Moehl, J. M. Gérard, and L. Ferlazzo, Appl. Phys. Lett. **87**, 233114 (2005).

[10] M. Rabe, M. Lowisch, and F. Heneberger, J. Cryst. Growth **184/185**, 102 (1998).

[11] E. Kurtz, J. Shen, M. Schmidt, M. Grün, S. K. Hong, D. Litvinov, D. Gerthen, T. Oka, T. Yao, and C. Klingshirn, Thin Solid Films **367**, 68 (2000).

[12] K. Leonardi, D. Hommel, C. Meyne, J. T. Zettler, and W. Richter, J. Cryst. Growth **201/202**, 1222 (1999).

[13] F. Gindele, U. Woggon, W. Langbein, J. M. Hvam, K. Leonardi, D. Hommel, and H. Selke, Phys. Rev. B **60**, 8773 (1999).

[14] S. V. Ivanov, A. A. Toropov, T. V. Shubina, A. V. Lebedev, I. V. Sedova, P. S. Kop'ev, G. R. Pozina, J. P. Bergman, and B. Monemar, J. Appl. Phys. **83**, 3168 (1998).

[15] T. Passow, K. Leonardi, H. Heinke, D. Hommel, D. Litvinov, A. Rosenauer, G. Gerthsen, J. Seufert, G. Bacher, and A. Forchel, J. Appl. Phys. **92**, 6546 (2002).

[16] T. Passow, H. Heinke, T. Schmidt, J. Falta, A. Stockmann, H. Selke, P. L. Ryder, K. Leonardi, and D. Hommel, Phys. Rev. B **64**, 193311 (2001).

[17] I. C. Robin, R. André, H. Mariette, S. Tatarenko, L. S. Dang, J. Bleuse, E. Bellet-Amalric, and J. M. Gérard, Nanotechnology **16**, 1116 (2005).

[18] I. C. Robin, R. André, C. Bougerol, T. Aichele, and S. Tatarenko, Appl. Phys. Lett. **88**, 233103 (2006).

[19] I. C. Robin, R. André, H. Mariette, S. Tatarenko, L. S. Dang, J. M. Gérard, and E. Bellet-Amalric, Physica E (Amsterdam) **26**, 119 (2005).

[20] R. Pässler, Phys. Status Solidi B **216**, 975 (1999).

[21] C. Bougerol, R. André, I. C. Robin, B. Gilles, B. van Daele, and G. van Tendeloo, Phys. Status Solidi C **3**, 938 (2006).

[22] N. Peranio, A. Rosenauer, D. Gerthsen, S. V. Sorokin, I. V. Sedova, and S. V. Ivanov, Phys. Rev. B **61**, 16015 (2000).

[23] L. C. Andreani, *Confined Electrons and Photons* (Plenum, New York, 1995), p. 57.

[24] J. M. Gérard and B. Gayral, *Confined Photon Systems Fundamentals and Applications* (Springer, New York, 1998), p. 331.

[25] E. O. Kane, J. Phys. Chem. Solids **1**, 249 (1957).

[26] M. Cardona, J. Phys. Chem. Solids **24**, 1543 (1963).

[27] B. P. Zhang, D. D. Manhand, K. Wakatsuki, and Y. Segawa, Appl. Phys. Lett. **77**, 3950 (2000).

[28] S. Yamaguchi, H. Kurusu, Y. Kawakami, S. Fujita, and S. Fujita, Phys. Rev. B **61**, 10303 (2000).

[29] M. Sugawara, Phys. Rev. B **51**, 10743 (1995).

[30] L. C. Andreani, Solid State Commun. **77**, 641 (1991).

[31] H. Gotoh, H. Ando, and T. Takagahara, J. Appl. Phys. **81**, 1785 (1997).

[32] H. Akiyama, S. Koshiba, T. Someya, K. Wada, H. Noge, Y. Nakamura, T. Inoshita, A. Shimizu, and H. Sakaki, Phys. Rev. Lett. **72**, 924 (1994).

[33] B. Patton, W. Langbein, and U. Woggon, Phys. Rev. B **68**, 125316 (2003).

[34] M. Gurioli, A. Vinattieri, M. Colocci, C. Deparis, J. Massies, G. Neu, A. Bosacchi, and S. Franchi, Phys. Rev. B **44**, 3115 (1991).

[35] M. Gurioli, J. Martinez-Pastor, M. Colocci, C. Deparis, B. Chastaingt, and J. Massies, Phys. Rev. B **46**, 6922 (1992).

[36] L. Marsal, L. Besombes, F. Tinjod, K. Kheng, A. Wasiela, B. Gilles, J. L. Rouvière, and H. Mariette, J. Appl. Phys. **91**, 4936 (2002).

[37] G. V. Astakhov, V. P. Kochereshko, D. R. Yakovlev, W. Ossau, J. Nürnberger, W. Faschinger, and G. Landwehr, Phys. Rev. B **62**, 10345 (2000).

[38] P. Kelkar, V. Kozlov, H. Jeon, A. V. Nurmikko, C. C. Chu, D. C. Grillo, J. Han, C. G. Hua, and R. L. Gunshor, Phys. Rev. B **52**, R5491 (1995).

[39] S. Moehl, L. Maingault, K. Kheng, and H. Mariette, Appl. Phys. Lett. **87**, 033111 (2005).

[40] P. Hawrylak, Phys. Rev. B **60**, 5597 (1999).